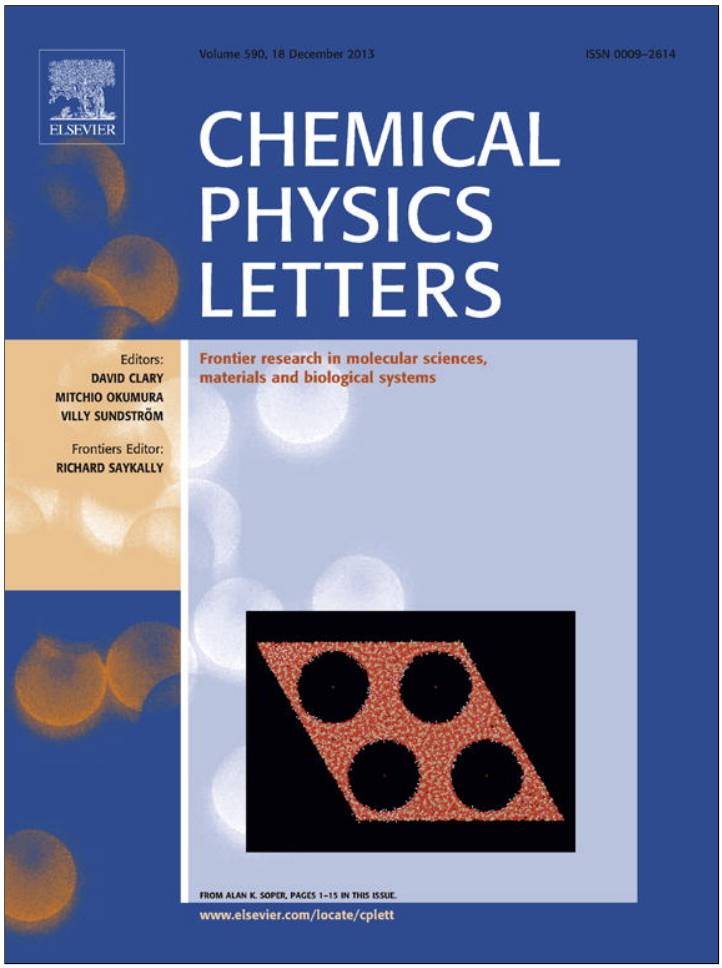

Chemical Physics Letters 590 (2013) 121–125

Contents lists available at ScienceDirect

Chemical Physics Letters

journal homepage: www.elsevier.com/locate/cplett

Graphene–carbon nanotube composite aerogel for selective detection of uric acid

Feifei Zhang [a,b,c], Jie Tang [a,b,*], Zonghua Wang [c], Lu-Chang Qin [d,*]

[a] National Institute for Materials Science, 1-2-1 Sengen, Tsukuba 305-0047, Japan
[b] Doctoral Program in Materials Science and Engineering, University of Tsukuba, Tsukuba 305-8577, Japan
[c] Laboratory of Fiber Materials and Modern Textile, Qingdao University, Qingdao, Shandong 266071, China
[d] Department of Physics and Astronomy, University of North Carolina at Chapel Hill, Chapel Hill, NC 27 599, USA

ARTICLE INFO

Article history:
Received 1 September 2013
In final form 21 October 2013
Available online 29 October 2013

ABSTRACT

Graphene and single-walled carbon nanotube (SWNT) composite aerogel has been prepared by hydrothermal synthesis. The restacking of graphene is effectively reduced by SWNTs inserted in between graphene layers in order to make available more active sites and reactive surface area. Electrochemical experiments show that the graphene–SWNT composite electrode has superior catalytic performance in selective detection of uric acid (UA).

1. Introduction

Nanostructured carbon has been widely used in electro-analysis and electro-catalysis. For example, carbon nanotubes (CNTs) have shown excellent performance in biosensors, chemical sensors, and biofuel cells [1,2]. CNT-based electrodes also showed electrocatalytic properties in the oxidation/reduction of a wide variety of compounds [3]. CNTs are very useful for electrochemical sensing because of their high surface area and rigid structure, which enabled construction of truly 'nanoarchitec-tonic' electrodes [4].

Graphene has attracted significant research interest in recent years. It's intriguing physicochemical properties, including large specific surface area (theoretically 2630 $m^2 g^{-1}$) [5], extraordinary electronic properties [6], superior chemical stability [5], and excellent thermal and electrical conductivities [7,8], made possible many applications in electrochemical devices such as chemical sensors, biosensors, supercapacitors, and batteries [9–11]. For electrochemical sensing, for example, the high surface area of graphene can give rise to high densities of attached analytic molecules, which in turn can facilitate high sensitivity and device miniaturization. The facile electron transfer between graphene and redox species opens up opportunities for sensing strategies that can be based on direct electron transfer rather than mediation. As a result, graphene has already revealed potential applications in electrochemistry, and remarkably rapid progress in this area has already been made [12].

A number of experimental methods have been developed for preparation of graphene, including mechanical exfoliation, chemical vapor deposition (CVD), hydrothermal synthesis, and chemical oxidation-reduction [13]. Hydrothermal synthesis is an efficient and non-toxic method for large-scale production without using any chemical reagents or catalysts. However, graphene sheets tend to aggregate irreversibly through the strong π–π interactions during the reduction process, thereby decreasing the effective specific surface area. One feasible proposal has been to use spacers to avoid or reduce the restacking and agglomeration of graphene. On the other hand, it would apparently be a better choice if the selected spacers could also contribute to the specific surface area, stability, and reactivity of the electrode material and structure.

Uric acid is an important analyte of clinical interest (normal level in serum 4.0−8.8 mg dL^{-1}, its early detection can be helpful to prevent various diseases like kidney stone, gout, diabetes, and cardiovascular disease [14,15]). Current methods for detection of UA include enzymatic-based assay [16], capillary electrophoresis [17], high performance liquid chromatography [18], and electrochemical techniques [19]. Among those methods, the electrochemical method is the most rapid, economical, and convenient one. But one of the major problems in biological determination of UA comes from electrochemical interferences from substance such as ascorbic acid (AA) and dopamine (DA), which have a similar oxidation potential at normal electrodes.

In this Letter, we describe the preparation and processing of graphene and single-walled carbon nanotubes (SWNTs) composite (hydrothermal G/S) by a hydrothermal method, where the SWNTs are connected with graphene and also inserted into the interlayer space between graphene sheets to reduce restacking of graphene. The G/S composite modified galssy carbon electrode (GCE) has also been fabricated and explored for selected detection of uric acid (UA).

* Corresponding authors. National Institute for Materials Science, 1-2-1 Sengen, Tsukuba 305-0047, Japan. Fax: +1 919 962 0480.
E-mail addresses: tang.jie@nims.go.jp (J. Tang), lcqin@email.unc.edu (L.-C. Qin).

0009-2614/$ - see front matter © 2013 Elsevier B.V. All rights reserved.
http://dx.doi.org/10.1016/j.cplett.2013.10.058

2. Experimental

2.1. Hydrothermal synthesis of graphene/SWNT composite

Graphene oxide (GO) was obtained from graphite by a modified Hummers–Offeman method, which was developed and used in our previous work for supercapacitor applications [20]. Atomic force microscopy (AFM) measurement indicated that the GO nanosheets were mostly of a monolayer structure with thickness of about 0.8 nm.

In order to remove the catalyst impurities, 50 mg SWNTs were sonicated for 5 h in 200 ml of an acid mixture (100 ml 48% HF and 100 ml 98% HNO_3, in the presence of SDS). The resulting dispersion was filtered and rinsed twice with 200 ml deionized water of pH 12 (adjusted by addition of sodium hydroxide), followed by rinsing with 800 ml methanol and then vacuum dried at 100 °C for 16 h. The product is termed as a-SWNTs hereafter [21].

Solutions of GO and a-SWNTs with respective concentration of 1 and 0.25 mg ml^{-1} were mixed together and then sealed in a 200 ml Teflon-lined autoclave for 4 h at 180 °C to obtain hydrothermal graphene-SWNT composite (hydrothermal G/S) hydrogel after it was freeze dried for 48 h. For comparison studies, hydrothermally reduced graphene oxide (hydrothermal G) without adding a-SWNTs was also prepared by the same process.

In the synthetic process of hydrothermal G/S composite (Figure 1), GO and a-SWNTs were both negatively charged when they were dispersed in water, as a result of ionization of the carboxylic acid and phenolic hydroxyl groups that are known to exist on the GO sheets, SWNT tips, and SWNT surface during oxidation. Therefore, GO and a-SWNTs can be well dispersed by electrostatic repulsions. When this suspension is reduced by hydrothermal treatment, there are several possible reactions to take place between GO and SWNTs: (1) elimination of OH and H can occur on the edge sites of graphene, resulting the recovery of π-conjugation, which believed to be analogous to the H^+-catalyzed dehydration of alcohol [22]; (2) in the meanwhile, intermolecular dehydration can occur on the edges or basal planes of graphene and tips or surface of SWNTs by cross-linking of hydroxyl and carboxylic groups; and (3) carbon dioxide is released during thermal treatment due to the reduction of linearly clustered epoxy groups and leases vacancies and topological defects on the carbon plate [23]. These three factors together with the π-stacking of graphene sheets and SWNTs resulted in successful production of the hydrothermal G/S composite.

2.2. Characterization

Morphology and structure of the material were characterized using transmission electron microscopy (TEM; JEOL JEM-2100, operated at 90 kV), scanning electron microscopy (SEM, JEOL JSM-7001F), and atomic force microscopy (AFM, Agilent PicoScan). X-ray diffraction (XRD) was carried out using Rigaku RINT 2500 with Cu K_α radiation source. The specific surface area and pore size distribution were measured with AUTOSORB-1 (Quantachrome Instruments). X-ray photoelectron spectroscopy (XPS) measurements were made with a PHI Quantera SXM (ULTRAVAC-PHI).

2.3. Electrochemical measurements

Electrochemical measurements were performed using an Ivium CompactStat (Ivium Technologies B.V.). Bare or modified glassy carbon electrode (GCE) of 3 mm in diameter was used as the working electrode, platinum wire as the counter electrode, and saturated calomel electrode (SCE) as the reference electrode. GCEs were polished with alumina slurry (0.05 and 0.3 μm) on a polishing cloth, then cleaned in acetone and distilled water bath with sonication for 5 min and finally rinsed with doubly distilled water. The clean electrode was dried under an infrared lamp. 10 mg of a-SWNTs, hydrothermal G, and hydrothermal G/S composite aerogel were dispersed for 30 min with the aid of ultrasonic agitation in 10 ml water to produce a solution with concentration of 1 mg ml^{-1}. An a-SWNT modified electrode (a-S/GCE), hydrothermal G modified electrode (H-G/GCE), and hydrothermal G/S composite modified electrode (H-G/S/GCE) were prepared by dropping 4 μL of the solution with a finnpipette on the GCE and then heated under an IR lamp to remove the liquid solution.

3. Results and discussion

The hydrothermal G/S composite has a well-defined and interconnected three-dimensional porous network as observed by SEM and TEM in the structure of its freeze-dried aerogel, shown in Figure 2. The SWNTs are inserted into the interlayer space of graphene and restacking of graphene could therefore be effectively prevented. At the same time, intra-pores would be created to increase the specific surface area and the analytic molecules would become more accessible to the electrode surface. Nitrogen-adsorption and -desorption isotherms are shown in Figure 3a. Using these isotherms, the multipoint Brunauer–Emmett–Teller (BET) specific surface areas of a-SWNTs, hydrothermal G, and hydrothermal G/S composite were obtained as 442, 483, and 656 $m^2 g^{-1}$, respectively. The BET specific surface area of the hydrothermal G/S composite is much larger than that of a-SWNTs and hydrothermal G. This fact indicates that the well-dispersed SWNTs acted indeed as spacers between the graphene layers, reduced the restacking of graphene sheets, and helped to produce a three-dimensional network structure with intra-pores. The pore size distribution obtained from density functional theory (DFT) model is shown in the inset of Figure 3b. Compared with hydrothermal G, pores with diameter of 3.8 nm in the hydrothermal G/S composite were

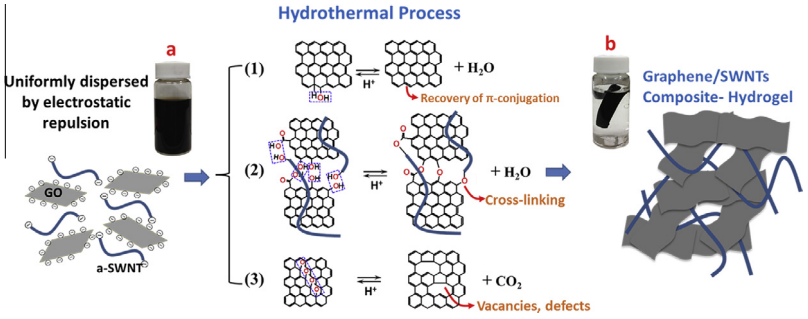

Figure 1. Mechanism of formation for hydrothermal reduction of graphene/SWNT composite. Inset a shows photograph of GO and a-SWNT dispersion and inset b shows photograph of hydrothermal G/S composite hydrogel in water.

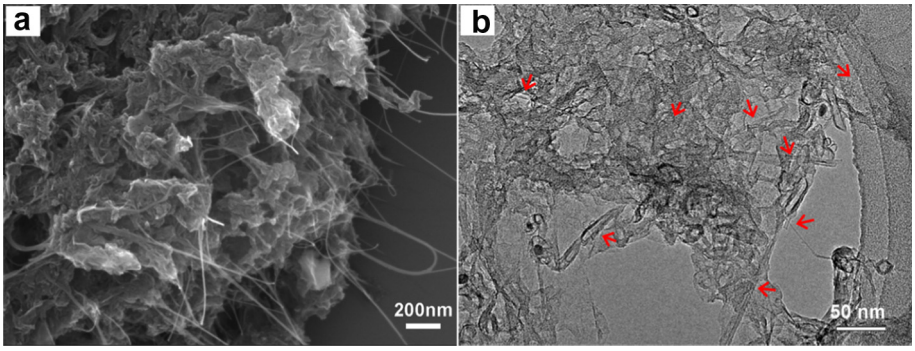

Figure 2. (a) SEM and (b) TEM image of hydrothermal G/S composite. Red arrows indicate SWNTs. (For interpretation of the references to color in this figure legend, the reader is referred to the web version of this article.)

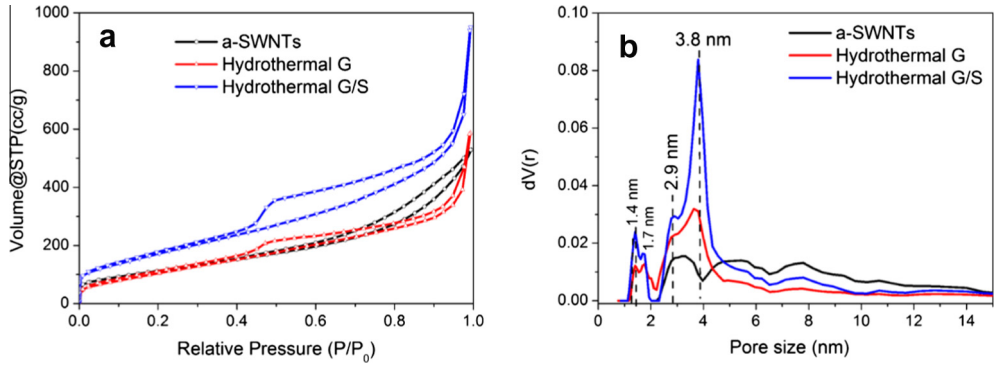

Figure 3. (a) Nitrogen-adsorption and -desorption isotherms and (b) DFT pore-size distribution of a-SWNTs (black), hydrothermal G (red), and hydrothermal G/S composite (blue). (For interpretation of the references to color in this figure legend, the reader is referred to the web version of this article.)

increased significantly, which can also contribute to the 'spacer' effect of SWNTs.

X-ray diffraction (XRD) patterns of graphite, graphene oxide, and hydrothermal G/S composite powders are shown in Figure 4. There is a broad and a narrow peak in the hydrothermal G/S composite with interlayer spacing of 0.37 nm. This value is much lower than that of GO (0.78 nm), but it is slight larger than that of graphite (0.34 nm). These results suggest that some π–π stacking of graphene sheets and also residual oxygenated functional groups were still present in the graphene/SWNT composite structure.

XPS was applied to determine the elemental composition as well as chemical and electronic states of elements on the surface of the material (Figure 5). The surface chemistry of modified electrodes is known to affect the electrochemical processes. For example, adsorption or chelation effects can arise from surface charges [24]. Figure 5a shows the wide spectra of GO and hydrothermal G/S composite. Using the C1s and O1s signal intensities, the C:O ratios were calculated to be 2.3 and 10.4 for GO and hydrothermal G/S composite, respectively, which clearly revealed that the GO and a-SWNTs solution were effectively reduced in the hydrothermal process.

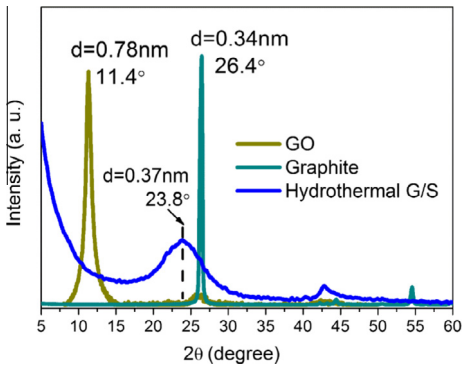

Figure 4. XRD patterns of graphite (dark cyan), GO (dark yellow), and hydrothermal G/S composite (blue). (For interpretation of the references to color in this figure legend, the reader is referred to the web version of this article.)

The high-resolution C1s spectra of GO and hydrothermal G/S composite are shown in Figure 5b. The peak at 284.3 eV corresponds to the sp^2 hybridized graphitic carbon and the peak at 290.7 eV corresponds to the π—π* structure. The peaks at 285.0, 287.0, and 288.4 eV are attributed to C—C, C—OH, and O—C=O, respectively [25]. Compared with GO, the spectra of the hydrothermal G/S composite had a dominant peak at 284.3 eV and two small peaks at 288.4 and 290.7 eV, corresponding to sp^2 C—C, O—C=O, and π—π* bonds, respectively, which clearly revealed that most of the oxygen groups had been removed. The peak of O—C=O configuration at 288.4 eV indicates the chemical bonding between graphene and SWNTs by cross-linking reactions.

To evaluate the electrochemical activity of the hydrothermal G/S composite for detection of UA, cyclic voltammograms (CV) were collected within the potential range from –0.2 to 0.8 V at scanning rate of 50 mV s^{-1}. The CVs of UA at H-G/S/GCE, H-G/GCE, a-S/GCE, and bare GCE are shown in Figure 6a. As can be seen, UA exhibits a broad and small CV peak in response at 0.47 V at the bare GCE and a-S/GCE and H-G/GCE led to an increasing anodic peak at the same potential. Since catalyst impurities in SWNTs have been removed in the acid treatment, the reason for the improved performance of a-S/GCE is attributed to the nanoscale dimensions of the structural elements, the electronic structure, and the topological defects present on the nanotube surface and tips. The enhanced oxidation current due to UA on H-G/GCE is attributed to the high density of defective sites at graphene edges, which provided many more active sites for electron transfer to the

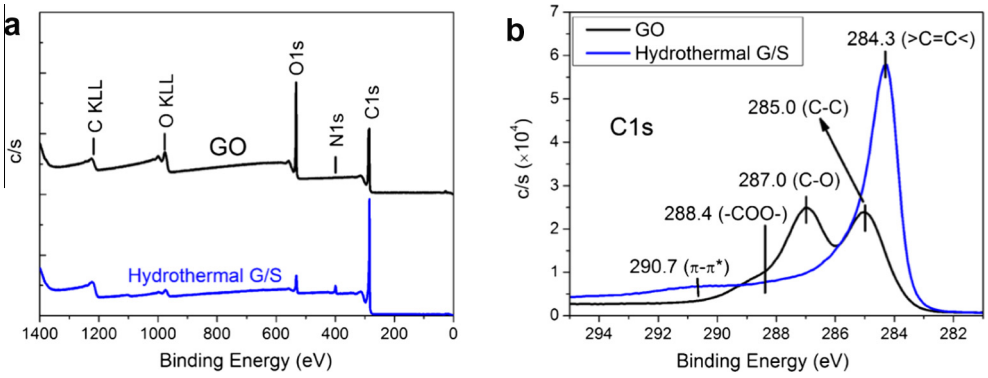

Figure 5. The XPS wide spectra (a), and high resolution C1s XPS spectra (b) of GO (black line) and hydrothermal G/S composite (blue line). (For interpretation of the references to color in this figure legend, the reader is referred to the web version of this article.)

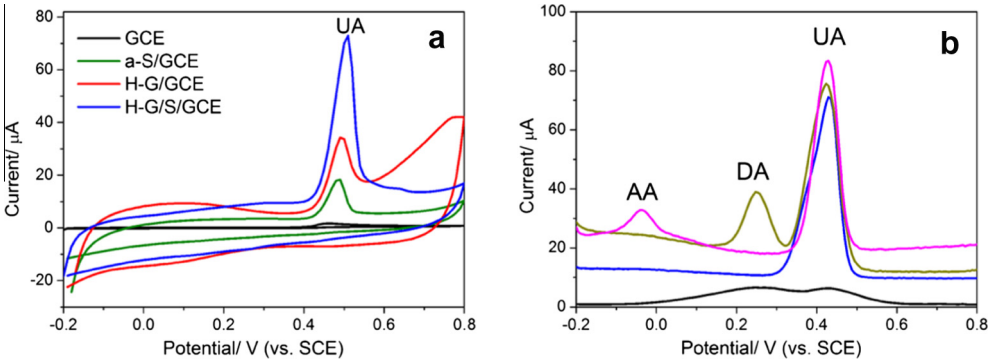

Figure 6. (a) CVs of 1.0×10^{-5} M UA at bare GCE (black), a-S/GCE (olive), H-G/GCE (red), and H-G/S/GCE (blue). (b) DPVs of a mixture of 1.0×10^{-5} M UA, 4.0×10^{-4} M AA, and 2.5×10^{-6} M DA at bare GCE (black); 1.0×10^{-5} M UA and 4.0×10^{-4} M AA (magenta), 1.0×10^{-5} M UA, and 2.5×10^{-6} M DA (dark cyan) and 1.0×10^{-5} M UA (blue) at H-G/S/GCE. (b) shows a series of differential pulse voltammograms (DPVs) of UA, ascorbic acid (AA), and dopamine (DA) mixture (DA and AA are typical interfering elements for electrochemical detection of UA, which coexist with UA in body fluid with similar oxidation potential on GCE). Only one rather broad, small, and overlay wave at 0.2–0.5 V appeared at the bare GCE (black curve). The current enhancement at H-G/S/GCE was remarkable and in addition, a decrease in the oxidation potential of AA occurred. AA, DA and UA can be distinguished from each other by a large anodic peak potential difference ($\Delta E_{p(UA,AA)}$ = 465 mV (magenta curve) and $\Delta E_{p(UA,DA)}$ = 180 mV (dark cyan curve)), which is large enough for selective determination of UA. In the buffer solution of pH 4.6, AA exists in an anionic form, while UA exists in a neutral form, since their pK_a values are 4.1 and 5.4, respectively. Neutral UA interacts more strongly with oxygen groups in graphene and SWNTs by hydrogen bonds. But HA^- (anionic form of AA) will be repelled by the negative charges remained in the composite. (For interpretation of the references to color in this figure legend, the reader is referred to the web version of this article.)

biological species [26]. The height of oxidation peak of UA at H-G/S/GCE is the highest, which means that the concentration of UA at H-G/S/GCE was higher than that at a-S/GCE and H-G/GCE. It can be explained that the effective insertion of SWNT spacers in the graphene/SWNT composite reduced restacking of graphene sheets and also produced additional intra-pores, resulting larger surface area and more porosity in the structure. In addition, as a result, more active sites and reaction area were also exposed to the oxidation of UA.

Figure 6b shows a series of differential pulse voltammograms (DPVs) of UA, ascorbic acid (AA), and dopamine (DA) mixture (DA and AA are typical interfering elements for electrochemical detection of UA, which coexist with UA in body fluid with similar oxidation potential on GCE). Only one rather broad, small, and overlay wave at 0.2–0.5 V appeared at the bare GCE (black curve). The current enhancement at H-G/S/GCE was remarkable and in addition, a decrease in the oxidation potential of AA occurred. AA, DA and UA can be distinguished from each other by a large anodic peak potential difference ($\Delta E_{p(UA,AA)}$ = 465 mV (magenta curve) and $\Delta E_{p(UA,DA)}$ = 180 mV (dark cyan curve)), which is large enough for selective determination of UA. In the buffer solution of pH 4.6, AA exists in an anionic form, while UA exists in a neutral form, since their pK_a values are 4.1 and 5.4, respectively. Neutral UA interacts more strongly with oxygen groups in graphene and SWNTs by hydrogen bonds. But HA^- (anionic form of AA) will be repelled by the negative charges remained in the composite.

The analytical determination experiments of UA were carried out using the DPVs for reducing the influence of background current. The oxidation peak current was related to the concentration of UA. A linear relationship between I_{pa} and the UA concentration was observed in the range of 2.5 and 65 μM (Figure 7, y = 9.9663 + 4.5648x, R = 0.9960) and the detection limit was established to be 0.5 μM (S/N = 3). The H-G/S/GCE retained 98% of its initial response after 2 weeks of storage in dry conditions. Such stability is acceptable for most practical applications.

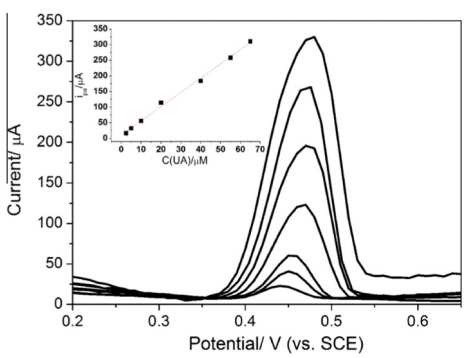

Figure 7. DPV recordings of UA at H-G/S/GCE. Inset: graph of oxidation peak current vs. UA concentration.

Table 1
Figures of merits of comparable methods for determination of uric acid.

Electrode	Detection range (linear) (μM)	Detection limit (μM)	Peak potential difference (mV)	Ref.
MWCNT-T/GCE	10–200	1	$\Delta E_{p(UA,AA)}$ = 353 $\Delta E_{p(UA,DA)}$ = 164	[19]
α-CD/CNT/CPE	5.0–40.0	5.0	$\Delta E_{p(UA,DA)} \approx 130$	[27]
PDDA-AuNPs-GNs/GCE	0.5–20	0.1	$\Delta E_{p(UA,AD)}$ = 170	[28]
GC/HDA/ERGO electrode	5–1000	0.08	$\Delta E_{p(UA,XA)}$ = 370 $\Delta E_{p(UA,HX)}$ = 710	[29]
Poly(L-arginine)/graphene	0.10–10.0	0.05	$\Delta E_{p(UA,XA)}$ = 390 $\Delta E_{p(UA,HX)}$ = 760	[30]
H-G/S/GCE	2.5–65	0.1	$\Delta E_{p(UA,AA)}$ = 465 $\Delta E_{p(UA,DA)}$ = 180	This work

The reproducibility was measured with the same electrode, and the relative standard deviation (RSD) was 0.8% (n = 5). When the modified electrode was prepared repeatedly five times, the RSD was 1.5%.

Table 1 lists the determined parameters of this modified electrode in comparison with other modified electrodes that are often used for the determination of UA. Compared with the literature reports on the determination of UA [19,27–30], the hydrothermal graphene/SWNT composite modified electrode showed excellent performance with a wider linear range, larger peak potential difference, and lower detection limit.

4. Conclusions

We have developed a graphene/SWNT composite aerogel by an efficient and non-toxic hydrothermal synthesis. Structural characterization using SEM, TEM, BET, and XRD suggest that the composite structure having SWNTs effectively inserted between the graphene layers. The graphene/SWNT composite modified electrode has been successfully utilized in the selective detection of UA, eliminating the interference of AA and DA. The composite modified electrode shows excellent linearity from 2.5 to 65 μM, lower detection limit of 0.1 μM, and sustaining stability for two weeks.

Acknowledgments

This Letter was supported by the JST ALCA Program, JSPS and NSFC under the Japan-China Scientific Cooperation Program (21111140014), JSPS Grants-in-Aid for Scientific Research 22310074, and the MEXT Nanotechnology Network Project, Japan.

References

[1] L. Agui, P. Yanez-Sedeno, J.M. Pingarron, Anal. Chim. Acta 622 (2008) 11.
[2] K.P. Gong, Y.M. Yan, M.N. Zhang, L. Su, S.X. Xiong, L.Q. Mao, Anal. Sci. 21 (2005) 1383.
[3] M.D. Rubianes, G.A. Rivas, Electrochem. Commun. 9 (2007) 480.
[4] M. Pumera, Chem-Eur. J. 15 (2009) 4970.
[5] A.K. Geim, K.S. Novoselov, Nat. Mater. 6 (2007) 183.
[6] K.S. Novoselov, Z. Jiang, Y. Zhang, S.V. Morozov, H.L. Stormer, U. Zeitler, J.C. Maan, G.S. Boebinger, P. Kim, A.K. Geim, Science 315 (2007) 1379.
[7] A.A. Balandin, S. Ghosh, W.Z. Bao, I. Calizo, D. Teweldebrhan, F. Miao, C.N. Lau, Nano Lett. 8 (2008) 902.
[8] K.I. Bolotin, K.J. Sikes, Z. Jiang, M. Klima, G. Fudenberg, J. Hone, P. Kim, H.L. Stormer, Solid State Commun. 146 (2008) 351.
[9] X. Huang, Z.Y. Zeng, Z.X. Fan, J.Q. Liu, H. Zhang, Adv. Mater. 24 (2012) 5979.
[10] Y.Y. Shao, J. Wang, H. Wu, J. Liu, I.A. Aksay, Y.H. Lin, Electroanalysis 22 (2010) 1027.
[11] Y. Wang, Y. Li, L. Tang, J. Lu, J. Li, Electrochem. Commun. 11 (2009) 889.
[12] D. Chen, H.B. Feng, J.H. Li, Chem. Rev. 112 (2012) 6027.
[13] X.Y. Yuan, J. Inorg. Mater. 26 (2011) 561.
[14] M.H. Alderman, Ann. Intern. Med. 132 (2000) 591.
[15] D. Lakshmi, M.J. Whitcombe, F. Davis, P.S. Sharma, B.B. Prasad, Electroanalysis 23 (2011) 305.
[16] N.C.M. Zanon, O.N. Oliveira Jr, L. Caseli, J. Colloid Interface Sci. 373 (2012) 69.
[17] C.D. Georgakopoulos, F.N. Lamari, I.N. Karathanasopoulou, V.S. Gartaganis, N.M. Pharmakakis, N.K. Karamanos, Biomed. Chromatogr. 24 (2010) 852.
[18] X.H. Dai, X. Fang, C.M. Zhang, R.F. Xu, B. Xu, J. Chromatogr. B 857 (2007) 287.
[19] H.Q. Bi, Y.H. Li, S.F. Liu, P.Z. Guo, Z.B. Wei, C.X. Lv, J.Z. Zhang, X.S. Zhao, Sens. Actuator B-Chem. 171 (2012) 1132.
[20] Q. Cheng, J. Tang, J. Ma, H. Zhang, N. Shinya, L.-C. Qin, J. Phys. Chem. C 115 (2011) 23584.
[21] D. Chattopadhyay, I. Galeska, F. Papadimitrakopoulos, Carbon 40 (2002) 985.
[22] Y. Zhou, Q.L. Bao, L.A.L. Tang, Y.L. Zhong, K.P. Loh, Chem. Mat. 21 (2009) 2950.
[23] H.C. Schniepp, J.L. Li, M.J. McAllister, H. Sai, M. Herrera-Alonso, D.H. Adamson, R.K. Prud'homme, R. Car, D.A. Saville, I.A. Aksay, J. Phys. Chem. B 110 (2006) 8535.
[24] C.H. An Wong, A. Ambrosi, M. Pumera, Nanoscale 4 (2012) 4972.
[25] Y. Li, Y. Zhao, H. Cheng, Y. Hu, G. Shi, L. Dai, L. Qu, J. Am. Chem. Soc. 134 (2011) 15.
[26] C.E. Banks, T.J. Davies, G.G. Wildgoose, R.G. Compton, Chem. Commun. 7 (2005) 829.
[27] S.M. Ghoreishi, M. Behpour, M.H.M. Fard, J. Solid State Electrochem. 16 (2012) 179.
[28] Y. Xue, H. Zhao, Z.J. Wu, X.J. Li, Y.J. He, Z.B. Yuan, Biosens. Bioelectron. 29 (2011) 102.
[29] M.A. Raj, S.A. John, Anal. Chim. Acta 771 (2013) 14.
[30] F.Y. Zhang, Z.H. Wang, Y.Z. Zhang, Z.X. Zheng, C.M. Wang, Y.L. Du, W.C. Ye, Talanta 93 (2012) 320.